Outstanding Thermal Conductivity of Single Atomic Layer Isotope-Modified Boron Nitride

Outstanding thermal conductivity of single atomic layer isotope-modified boron nitride

Waste heat dissipation in highly integrated and miniaturized modern devices is a great challenge,[1,2] and electrically insulating materials of high thermal conductivity (κ) provide the solution. Herein, we report that one atomic layer (1L) isotopically pure hexagonal boron nitride (*h*BN) is one of the best thermal conductors among all semiconductors and electric insulators. It has a κ up to 1009 W/mK at room temperature, 34% and 140% higher than those of 1L and bulk naturally occurring *h*BN, respectively. The isotope engineering minimizes isotopic disorder, and reducing the thickness to one atomic layer diminishes the interlayer interactions, both of which greatly decrease phonon scattering and enhance κ. This κ value is comparable to that of the recently discovered cubic boron arsenide (BAs),[3-5] but with its layered structure, mechanical flexibility and strength, and low density, 1L monoisotopic BN is more promising on heat management in van der Waals (vdW) devices and future flexible electronics. The isotope engineering of atomically thin BN may also open up other appealing applications and opportunities in 2D materials yet to be explored.

A dramatic temperature rise can occur locally at the so-called "hot spot" in highly integrated and miniaturized devices, including microprocessor and circuit packages, light-emitting diodes, high-power lasers and radio frequency transmitters. Eliminating waste heat limits the performance, reliability, and longevity of many modern devices. Materials with outstanding thermal conductivities (κ) can provide the solution to this challenge. While diamond and graphite are the only two traditional materials with κ above 1000 W/mK at room temperature, emerging materials such as carbon nanotubes,[6] graphene,[7] and recently discovered cubic

boron arsenide (cBAs) (~1000 W/mK)[3-5] are also excellent thermal conductors. However, carbon materials are not suitable in direct contact with electronic devices due to the potential for short circuiting caused by their electric conductivity. In addition, diamond and cBAs are expensive and unbendable, making them unsuitable for flexible electronic devices and new two-dimensional (2D) van der Waals (vdW) structures.

Distinct from their carbon counterparts, all boron nitride (BN) materials, including single-wall nanotubes and one atomic layer or monolayer (1L) BN are electric insulators and hence better candidates for waste heat dissipation, for example, in electronic devices. Bulk cubic and hexagonal BN crystals are good thermal conductors with κ of ~690 and 420 W/mK at room temperature, respectively.[8] Recently, it was reported that high-quality and surface-clean 1L *h*BN had a κ of 751±340 W/mK.[9] This κ increase with reduced thickness down to the atomic level was due to a decrease in the number of phonon branches and states available for Umklapp scattering with less interlayer interaction. Defects, grain boundaries, and surface contaminations, nevertheless, could adversely affect the thermal conduction of atomically thin BN.[10-14]

Isotope engineering affects many fundamental properties of a solid, *e.g.* lattice parameter, disordering, elastic constant, vibration, band structure and transition, exciton, polariton dispersion and scattering. It, in turn, gives rise to appealing phenomena and applications, including the elevation of superconducting transition temperature, improvement in the lifetime of organic light-emitting diodes (OLED), optical fibers with higher speed, precise and accurate quantification of proteomes, and ultra-trace environmental analysis. Naturally occurring BN (^{Nat}BN) contains a relatively high percentage of two stable boron isotopes: 19.9% ^{10}B and 80.1% ^{11}B; while carbon (C) normally consists of 98.9% ^{12}C and only 1.1% ^{13}C. The

phonon energy, electronic bandgap, and electron density distribution of *h*BN could be varied by isotope engineering.[15] Isotope enriched *h*BN greatly increased polariton lifetime.[16] In addition, ^{10}B is one of the best neutron absorbers and used widely in radiation shielding, nuclear reactivity control, and neutron capture therapy for tumor treatment. Replacing ^{10}B by ^{11}B, on the other hand, prevents electronic devices from data loss or single-event upset caused by cosmic rays or their generation of ionizing particles.

Reducing isotopic disorder also increases thermal conductivity. The in-plane κ of isotopically pure ^{12}C graphene is 36% and ~100% higher than that of naturally occurring graphene and graphite, respectively.[17] The κ of 1L isotopically pure $^{100}MoS_2$ were 61.6 W/mK, larger than the 40.8 W/mK of 1L $^{Nat}MoS_2$.[18] Note that chemical vapor deposition (CVD) was used to synthesize these monoisotopic graphene and MoS_2. In terms of BN, the room temperature κ of bulk ^{10}BN crystals was 585 W/mK, ~39% higher than that of bulk ^{Nat}BN.[19] The effect of isotopic impurity on the κ of BN nanotubes was also studied: 310 W/mK for ^{11}BN nanotubes, much larger than the 200 W/mK of ^{Nat}BN nanotubes as a control.[20] There has been no report on the synthesis of atomically thin monoisotopic BN, let alone measurement of its κ, though a 25-36% enhancement in κ was theoretically predicted from 1L isotopically pure BN compared to that of 1L ^{Nat}BN.[21-24]

In this work, we successfully produced atomically thin isotopically pure ^{10}BN and ^{11}BN for the first time, and their intrinsic in-plane thermal conductivities could be determined due to their high quality and clean surface. Based on optothermal Raman measurements, the κ of 1L ^{11}BN and ^{10}BN were 1009±313 and 958±355 W/mK, respectively. These values were ~34% and ~140% larger than those of 1L and bulk ^{Nat}BN, respectively. Density functional theory (DFT) simulations were used to gain insights into the isotope effect. Along with its wide

bandgap,[25] superb elasticity and strength,[26] excellent flexibility, and good chemical and thermal stability,[27] and compatibility with vdW heterostructure, atomically thin isotopically pure BN provides a new solution for the thermal management in next-generation electronics. It may also give rise to new possibilities in many other applications, *e.g.* multifunctional metal-matrix nanocomposites for radiation shielding and new cancer treatment.

Results and discussion

High-quality and surface-clean atomically thin isotopically pure BN sheets were mechanically exfoliated from bulk crystals grown by the nickel-chromium solvent method.[15,28] According to secondary ion mass spectrometry (SIMS), these bulk crystals contained 99.2% and 99.9% ^{10}B and ^{11}B, respectively, close to the previously reported values.[15] Naturally occurring nitrogen has >99.6% ^{14}N, and thus can be considered as isotopically pure. The atomically thin ^{10}BN and ^{11}BN sheets were directly exfoliated and suspended over pre-fabricated micro-wells (3.8 μm in diameter) connected by narrow trenches (200 nm in width) in 80 nm gold-coated Si substrates (Au/Si) without polymer-assisted transfer process. The Au films served as heat sinks during measurements; the trench acted as vents to avoid strain induced to the atomically thin materials due to volume change of the air trapped in the micro-wells during heating.

Fig. 1a and b show the atomic force microscopy (AFM) image and height trace of a suspended 1L ^{10}BN with a thickness of 0.50 nm. More samples and their AFM images are shown in Supplementary Materials (Fig. S1). The chemical composition, crystal structure, and quality of the isotopically pure samples were probed by near-edge X-ray absorption fine structure (NEXAFS) spectroscopy, and compared with those of a single crystal ^{Nat}BN synthesized by the high pressure Ba-BN solvent method (Fig. 1c).[29] Sharp π* resonances at

192.0 eV corresponding to 1*s* core electron transitions to the unoccupied antibonding orbitals of B atoms sp^2-bond to three nitrogen atoms were observed from all samples, verifying their hexagonal crystal structure. No satellite peaks caused by other chemical environments were present, suggesting high chemical purities of the isotopically pure samples.[30,31] These results are in line with the previous finding that the ^{10}BN and ^{11}BN crystals were free of defects in the areas of tens of microns.[19]

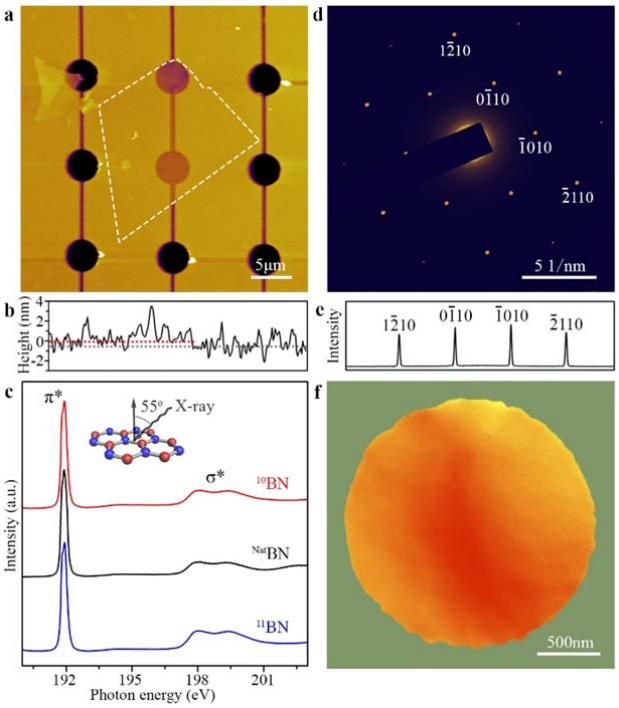

Fig. 1. Samples and characterisations. (a) AFM image of a mechanically exfoliated 1L ^{10}BN suspended over Au/Si substrate with micro-wells and trenches; (b) AFM height of the 1L sample; (c) NEXAFS spectra in the B K-edge region of isotopically pure and natural BN at the incidence of 55°; (d) selected area electron diffraction of a suspended 1L ^{10}BN; (e) the corresponding diffraction spot intensities; (f) the DF-TEM image.

Transmission electron microscope (TEM) was used to detect whether the exfoliated atomically thin sheets contained any grain boundary. Fig. 1d shows a typical electron diffraction pattern from the entire suspended area of a 1L ^{10}BN on perforated silicon nitride

(SiN_x) TEM grid with 2 μm holes. The diffraction pattern consisted of single sets of diffraction dots with six-fold symmetry. The intensity profile of the $(1\bar{2}10)$, $(0\bar{1}10)$, $(\bar{1}010)$ and $(\bar{2}110)$ diffraction reflections is plotted in Fig. 1e, which can be compared with those of 2L and few-layer samples shown in Supplementary Information, Fig. S2. The dark field (DF)-TEM image also revealed a mono-crystalline nature without grain boundaries (Fig. 1f). The TEM results of a 1L ^{11}BN are available in Supplementary Materials (Fig. S3).

Fig. 2a compares the Raman spectra of suspended 1-3L and bulk ^{10}BN, ^{Nat}BN and ^{11}BN. Since the Raman frequency is inversely proportional to the square root of mean atomic mass, the bulk ^{10}BN, ^{Nat}BN, and ^{11}BN crystals showed G bands centered at 1392.0, 1366.9, and 1358.0 cm^{-1}, respectively. Reducing the thickness of suspended monoisotopic BN to the atomic scale barely changed their G band Raman frequencies but lowered the peak intensities. A similar phenomenon on atomically thin ^{Nat}BN was reported and explained by us before.[27,32] Due to mass disorder effects, the different isotope mass also affected the full width at half maximum (FWHM) of the G bands of bulk ^{10}BN, ^{Nat}BN, and ^{11}BN crystals, *i.e.* 5.9, 9.4, and 5.6 cm^{-1}, respectively.[33] The atomically thin sheets showed broader bandwidths, caused by stronger surface scattering influencing the vibrational excitation lifetime.[27,32]

The κ of atomically thin ^{10}BN and ^{11}BN was measured by optothermal Raman technique.[7,9,18,34-38] First, the Raman G band frequency of the suspended 1L ^{10}BN and ^{11}BN as a function of temperature was determined using a hot plate with accurate temperature control (±0.1 °C). In order to minimize laser heating, a small laser power of ~1.5 mW was chosen. Fig. 2b summarizes the Raman G bands of a 1L ^{10}BN and ^{11}BN at 293-413 K with an interval of 10 K and the corresponding linear fittings, *i.e.* $\omega - \omega_0 = \chi T$, where χ is the first-order

temperature coefficient, and $\omega - \omega_0$ is the change of the G band frequency due to temperature variation. The χ values of 1L ^{10}BN and ^{11}BN were −0.0223±0.0008 (red dashed line in Fig. 2b) and −0.0220±0.0007 (blue dashed line) cm^{-1}/K, respectively, quite similar to that of ^{Nat}BN, *i.e.* −0.0223±0.0012 cm^{-1}/K (black dashed line).[9] Note that the volumetric thermal expansion of the Au/Si substrate during heating hardly affected these χ values due to the hanging down of suspended atomically thin BN, as it was described before.[9]

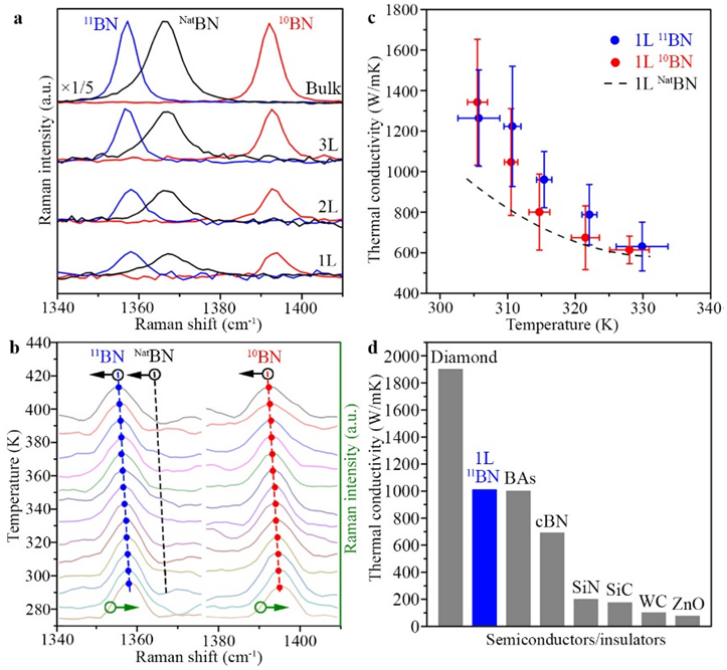

Fig. 2. Experimental thermal conductivity. (a) Comparison among Raman spectra of 1-3L and bulk ^{10}BN, ^{Nat}BN, and ^{11}BN; (b) temperature effect on the Raman G band frequency of 1L ^{10}BN, ^{Nat}BN and ^{11}BN sheets with corresponding fittings; (c) experimental κ of 1L ^{10}BN (red) and ^{11}BN (blue) as a function of temperature, compared with that of 1L ^{Nat}BN (black and dashed); (d) the comparison among κ of representative semiconductors and insulators.

The suspended 1L ^{10}BN and ^{11}BN sheets were then optically heated under different laser power (4-10 mW) to increase the local temperature (T_m) (see Supplementary Materials, Fig. S4 for the Raman spectra). Given that the heat flux vector is along the radial direction away

from the center of the suspended BN sheets and the phonon transport is diffusive, the thermal conductivity was calculated by:

$$\kappa = \frac{\ln(\frac{R}{r_0})}{2\pi d\frac{T_m - T_a}{Q - Q_{air}}}\alpha \qquad (1)$$

where R is the radius of the micro-well (1.9 μm); r_0 is the radius of the laser beam which was 0.32±0.01 μm (see Supplementary Materials, Fig. S5); α = 0.97 is the Gaussian profile factor of the laser beam; d is BN thickness; T_m is the temperature measured by Raman; T_a is the ambient temperature; Q is the absorbed laser power. The optical absorption of 1L ^{10}BN and ^{11}BN at 488 nm wavelength was determined by the difference in the measured laser power between empty and nearby BN-covered holes of SiN_x grids (see Supplementary Materials, Fig. S6). That is, $Q = P_{empty} - P_{BN}$. There was no noticeable difference in the absorbance of 1L ^{10}BN and ^{11}BN, and the averaged value was (0.32±0.13)%, close to that of 1L ^{Nat}BN.[9] Q_{air} is the heat loss in the air:

$$Q_{air} = \int_{r_0}^{R} 2\pi h(T - T_a) r dr + \pi r_0^2 h(T_m - T_a) \qquad (2)$$

where h is the heat transfer coefficient of *h*BN. In the case of small temperature variation between an object and the ambient, the quadratic expression for radiation can be simplified to the linearized sum of convective (h_c) and radiative (h_r) components to obtain the total heat transfer coefficient. That is, $h = h_c + h_r$, where h_c=3475W/m^{2}K for BN sheets; $h_r = \varepsilon\sigma 4T^3$; ε = 0.8 is the emissivity of *h*BN; and σ is the Stefan-Boltzmann constant with the value of 5.670373×10^{-8} W/m^{2}K^4.

The κ of 1L ^{10}BN and ^{11}BN as a function of temperature was calculated based on Equation 1, and compared with that of 1L ^{Nat}BN from previous study (Fig. 2c).[9] The errors were calculated through the root sum square error propagation approach, where the temperature calibration by Raman, temperature resolution of the Raman measurements, and the

uncertainty of the measured laser absorbance were considered. Due to the small temperature range and the uncertainty of the optothermal technique, we averaged the κ values: 958±355 and 1009±313 W/mK for 1L ^{10}BN and ^{11}BN near room temperature, respectively. Note optical heating was coupled more strongly to diffusive phonons of higher frequency than ballistic phonons, and the temperature measured by the Raman method was the anharmonic scattering temperature between the zone-center or zone-boundary optical phonons and diffusive acoustic phonons.[36,39,40] In addition, the local non-equilibrium of phonon polarizations was ignored.[41] As a result, these Raman-deduced κ values should be underestimated. Our results showed that the κ of 1L monoisotopic BN was about 34% and 140% higher than those of 1L ^{Nat}BN and bulk ^{Nat}BN, respectively.[8,9] Fig. 2d compares the κ of 1L ^{11}BN with those of some representative semiconductors and insulators.

Theoretical calculations were used to comprehensively understand the isotope effects. In the *ab initio* calculations of the κ of 1L ^{10}BN (99.2% ^{10}B), ^{Nat}BN, and ^{11}BN (99.9% ^{11}B), phonon-phonon, isotope, and boundary scatterings were taken into account. The boundary scattering rate was calculated as v_g/L, where v_g is the group velocity of the phonons, and L is the boundary length. Isotope mixing caused isotope scattering and shortened phonon mean free path (λ). At 4 μm length close to the experimental sample size, 99.9% ^{11}BN had slightly larger κ than 99.2% ^{10}BN (Fig. 3a), in excellent agreement with our experimental results. Our calculations also revealed that the isotope scattering mostly affected the out-of-plane optical (ZO) phonon branch in 1L BN, and the κ among 1L monoisotopic and natural BN deviated most dramatically at phonon frequencies of 600-850 cm^{-1} (Fig. 3b). Fig. 3c compares the κ of 1L BN with different ^{10}B concentrations, which followed a parabolic trend. For isotope scattering, $\lambda \propto g^{-1}T^{-4}$, where $g = \sum_i C_i \left[\left(M_i^2 - (\sum C_i M_i)\right)/(\sum C_i M_i)^2\right]^2$; T is the temperature; C_i and M_i are the concentration and mass of isotope atoms, respectively. g

reached its maximum at about 50% ^{10}B, resulting in the minimum λ and hence κ. Our theoretical κ values were larger than the experimental values and other theoretical predictions based on classical potentials (see Supplementary Materials, Table S1), and this could be due to the local density approximation (LDA). LDA is well known to over bind systems, leading to overestimations of phonon frequencies and consequently thermal conductivity.[42]

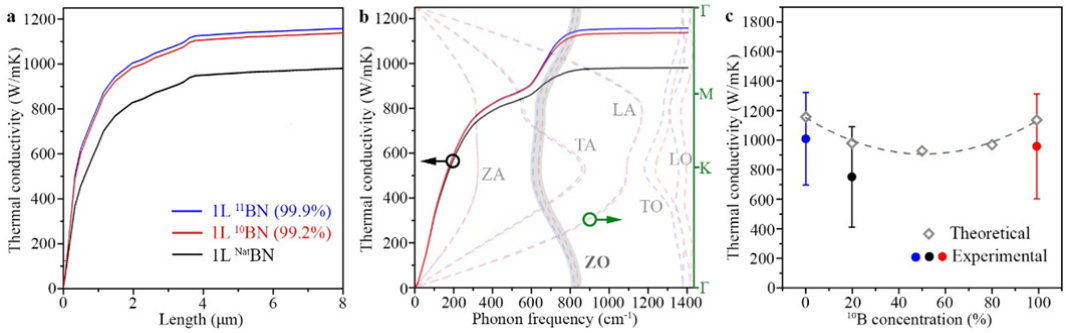

Fig. 3. Theoretical calculations. (a) Cumulative theoretical κ of 1L ^{10}BN, ^{11}BN, and ^{Nat}BN as a function of sample length; (b) cumulative theoretical κ of the same three materials as a function of phonon frequency, with the phonon dispersion of 1L ^{10}BN and ^{11}BN shown as the background and ZO phonon branches highlighted; (c) theoretical (open rhombus) and experimental (filled dots) κ of 1L BN as a function of ^{10}B concentration (*i.e.* 0.1%, 19.9%, 50%, 80%, and 99.2%), and corresponding parabolic fitting (dashed line).

Similar to the case of ^{Nat}BN reported before,[9] bilayer and trilayer monoisotopic BN had slightly smaller thermal conductivities than the corresponding monolayers, and the smaller κ values should be mainly caused by increased out-of-plane acoustic (ZA) phonon Umklapp scattering due to increased interlayer interactions (see Supplementary Materials, Fig. S7 and S8). This phenomena is similar in other 2D materials, *e.g.* graphene and MoS_2.[43,44]

Conclusions

In summary, high-quality and suspended atomically thin isotopically pure BN sheets were produced by mechanical exfoliation, and their intrinsic in-plane thermal conductivities were measured by the optothermal Raman technique: 958±355 and 1009±313 W/mK for 1L ^{10}BN and ^{11}BN at close-to room temperature, respectively. These values were about 34% and 140% larger than those of 1L and bulk ^{Nat}BN, respectively, attributed to 1) the longer mean free path of phonons due to less phonon-isotope scattering and 2) decreased phonon Umklapp scattering in atomically thin samples caused by less interlayer interactions and hence reduced phonon branches.

Methods

Sample fabrication and characterization. The trench-connected micro-wells were fabricated by the combination of photolithography and electron beam lithography (EBL). The depth of both the micro-wells and trenches was ~2 μm. The Au films on the Si substrates were coated by a metal sputter (Leica EM ACE600). The suspended atomically thin ^{10}BN and ^{11}BN was mechanically exfoliated on the Au/Si substrates by Scotch tape from bulk isotopically pure *h*BN crystals. Olympus BX51 and Asylum Research Cypher were used for optical microscopy and AFM. The NEXAFS measurements were performed in the ultrahigh vacuum chamber (~10^{-10} mbar) at the undulator soft x-ray spectroscopy beamline of the Australian Synchrotron. The Raman spectra were collected from A Renishaw inVia system equipped with a 488 nm laser, and a 100× objective lens with a numerical aperture of 0.90. All Raman spectra were calibrated by the band of Si at 520.5 cm^{-1}. The laser power that passed the objective lens was measured by an optical power meter (Newport 1916-C). The temperature was controlled with a heating stage (Linkam LTS350). SIMS analyses were performed on a CAMECA IMS 5FE7. For isotopic B contents, a focused 7.5 keV O_2^+ primary ion beam with a current of 3 nA was employed over ~15 μm in diameter area. TEM

was conducted on a JEOL 2100. For the optical absorption measurement, the atomically thin isotopic BN samples were firstly mechanically exfoliated onto 90 nm SiO_2 covered Si substrates and then transferred onto perforated SiN_x TEM grid by PMMA. The PMMA was removed by acetone and then acetic acid, followed by annealing at 450 ^{o}C in air.

Theoretical Calculations were carried out based on *ab initio* density functional theory employing the VASP[45,46] code. The local density approximation as parameterised by Perdew and Zunger[47] was used to model the exchange and correlation. The projector augmented wave method[48,49] was used in the description of the bonding environment for B and N. An energy cutoff of 1100 eV was used and electronic convergence was set to $1x10^{-9}$ eV. The atomic coordinates were allowed to relax until the forces on the ions were less than $5x10^{-7}$ eV/Å. The Brillouin zone was sampled with a 48×48×1 Γ-centered grid. Additionally, a dipole correction was applied across the cell along the non-periodic direction. Calculations on the phonon dispersion and Grüneisen parameter were carried out using Phonopy[50] and a 2×2×1 hexagonal cell. For the calculation of κ within the relaxation time approximation, Phono3py [51] was used along with an orthorhombic cell consisting of four primitive cells. An orthorhombic cell was employed as this significantly reduced the drift in the third-order force constants compared to a hexagonal cell. The orthorhombic cell was transformed back to the primitive cell using the matrix: (1/2 −1/4 0, 0 1/2 0, 0 0 1). In all calculations, a 35 Å vacuum spacing was used to limit spurious interactions along the non-periodic direction of the cell. Following *ab initio* calculations, this length was reduced to 3.335 Å to represent the interlayer spacing in bulk *h*BN. This was carried out due to the 1/Volume dependence in the calculation of κ. The cumulative thermal conductivity followed the definition in Ref. 52.[52]

References

1. Ball, P. Computer engineering: Feeling the heat. *Nature News* **492**, 174 (2012).

2. Waldrop, M. M. The chips are down for moore's law. *Nature News* **530**, 144 (2016).

3. Tian, F., et al. Unusual high thermal conductivity in boron arsenide bulk crystals. *Science* **361**, 582-585 (2018).

4. Li, S., et al. High thermal conductivity in cubic boron arsenide crystals. *Science* **361**, 579-581 (2018).

5. Kang, J. S., Li, M., Wu, H., Nguyen, H. & Hu, Y. Experimental observation of high thermal conductivity in boron arsenide. *Science* **361**, 575-578 (2018).

6. Berber, S., Kwon, Y. K. & Tomanek, D. Unusually high thermal conductivity of carbon nanotubes. *Phys. Rev. Lett.* **84**, 4613-4616 (2000).

7. Balandin, A. A., et al. Superior thermal conductivity of single-layer graphene. *Nano Lett.* **8**, 902-907 (2008).

8. Jiang, P. Q., Qian, X., Yang, R. G. & Lindsay, L. Anisotropic thermal transport in bulk hexagonal boron nitride. *Phys. Rev. Mater.* **2**, 064005 (2018).

9. Cai, Q., et al. High thermal conductivity of high-quality monolayer boron nitride and its thermal expansion. *Sci. Adv.* **5**, eaav0129 (2019).

10. Jo, I., et al. Thermal conductivity and phonon transport in suspended few-layer hexagonal boron nitride. *Nano Lett.* **13**, 550-554 (2013).

11. Alam, M. T., Bresnehan, M. S., Robinson, J. A. & Haque, M. A. Thermal conductivity of ultra-thin chemical vapor deposited hexagonal boron nitride films. *Appl. Phys. Lett.* **104**, 013113 (2014).

12. Zhou, H. Q., et al. High thermal conductivity of suspended few-layer hexagonal boron nitride sheets. *Nano Res.* **7**, 1232-1240 (2014).

13. Wang, C., et al. Superior thermal conductivity in suspended bilayer hexagonal boron nitride. *Sci. Rep.* **6**, 25334 (2016).

14. Lin, Z., Liu, C. & Chai, Y. High thermally conductive and electrically insulating 2D boron nitride nanosheet for efficient heat dissipation of high-power transistors. *2D Mater.* **3**, 041009 (2016).

15. Vuong, T., et al. Isotope engineering of van der Waals interactions in hexagonal boron nitride. *Nat. Mater.* **17**, 152 (2018).

16. Giles, A. J., et al. Ultralow-loss polaritons in isotopically pure boron nitride. *Nat. Mater.* **17**, 134 (2018).

17. Chen, S., et al. Thermal conductivity of isotopically modified graphene. *Nat. Mater.* **11**, 203 (2012).

18. Li, X., et al. Isotope-engineering the thermal conductivity of two-dimensional MoS_2. *ACS Nano* **13**, 2481-2489 (2019).

19. Yuan, C., et al. Modulating the thermal conductivity in hexagonal boron nitride via controlled boron isotope concentration. *Commun. Phys.* **2**, 43 (2019).

20. Chang, C., et al. Isotope effect on the thermal conductivity of boron nitride nanotubes. *Phys. Rev. Lett.* **97**, 085901 (2006).

21. Lindsay, L. & Broido, D. Enhanced thermal conductivity and isotope effect in single-layer hexagonal boron nitride. *Phys. Rev. B* **84**, 155421 (2011).

22. Dong, H., Hirvonen, P., Fan, Z. & Ala-Nissila, T. Heat transport in pristine and polycrystalline single-layer hexagonal boron nitride. *Phys. Chem. Chem. Phys.* **20**, 24602-24612 (2018).

23. Sevik, C., Kinaci, A., Haskins, J. B. & Çağın, T. Influence of disorder on thermal transport properties of boron nitride nanostructures. *Phys. Rev. B* **86**, 075403 (2012).

24. Lindsay, L. & Broido, D. Theory of thermal transport in multilayer hexagonal boron nitride and nanotubes. *Phys. Rev. B* **85**, 035436 (2012).

25. Li, L. H. & Chen, Y. Atomically thin boron nitride: Unique properties and applications. *Adv. Funct. Mater.* **26**, 2594-2608 (2016).

26. Falin, A., et al. Mechanical properties of atomically thin boron nitride and the role of interlayer interactions. *Nat. Commun.* **8**, 15815 (2017).

27. Li, L. H., Cervenka, J., Watanabe, K., Taniguchi, T. & Chen, Y. Strong oxidation resistance of atomically thin boron nitride nanosheets. *ACS Nano* **8**, 1457-1462 (2014).

28. Liu, S., et al. Single crystal growth of millimeter-sized monoisotopic hexagonal boron nitride. *Chem. Mater.* **30**, 6222-6225 (2018).

29. Taniguchi, T. & Watanabe, K. Synthesis of high-purity boron nitride single crystals under high pressure by using Ba-BN solvent. *J Cryst Growth* **303**, 525-529 (2007).

30. Caretti, I. & Jimenez, I. Point defects in hexagonal BN, BC_3 and BC_xN compounds studied by X-ray absorption near-edge structure. *J. Appl. Phys.* **110**, 023511 (2011).

31. Li, L. H., et al. High-resolution X-ray absorption studies of core excitons in hexagonal boron nitride. *Appl. Phys. Lett.* **101**, 191604 (2012).

32. Cai, Q. R., et al. Raman signature and phonon dispersion of atomically thin boron nitride. *Nanoscale* **9**, 3059-3067 (2017).

33. Carvalho, B. R., et al. Probing carbon isotope effects on the Raman spectra of graphene with different ^{13}C concentrations. *Phys. Rev. B* **92**, 125406 (2015).

34. Lee, J.-U., Yoon, D., Kim, H., Lee, S. W. & Cheong, H. Thermal conductivity of suspended pristine graphene measured by Raman spectroscopy. *Phys. Rev. B* **83**, 081419 (2011).

35. Cai, W., et al. Thermal transport in suspended and supported monolayer graphene grown by chemical vapor deposition. *Nano Lett.* **10**, 1645-1651 (2010).

36. Chen, S., et al. Raman measurements of thermal transport in suspended monolayer graphene of variable sizes in vacuum and gaseous environments. *ACS Nano* **5**, 321-328 (2010).

37. Zhou, H., et al. High thermal conductivity of suspended few-layer hexagonal boron nitride sheets. *Nano Research* **7**, 1232-1240 (2014).

38. Yan, R., et al. Thermal conductivity of monolayer molybdenum disulfide obtained from temperature-dependent Raman spectroscopy. *ACS Nano* **8**, 986-993 (2014).

39. Basko, D., Piscanec, S. & Ferrari, A. Electron-electron interactions and doping dependence of the two-phonon Raman intensity in graphene. *Phys. Rev. B* **80**, 165413 (2009).

40. Bonini, N., Lazzeri, M., Marzari, N. & Mauri, F. Phonon anharmonicities in graphite and graphene. *Phys. Rev. Lett.* **99**, 176802 (2007).

41. Vallabhaneni, A. K., Singh, D., Bao, H., Murthy, J. & Ruan, X. Reliability of Raman measurements of thermal conductivity of single-layer graphene due to selective electron-phonon coupling: A first-principles study. *Phys. Rev. B* **93**, 125432 (2016).

42. Perdew, J. P., et al. Atoms, molecules, solids, and surfaces-applications of the generalized gradient approximation for exchange and correlation. *Phys. Rev. B* **46**, 6671-6687 (1992).

359 43. Ghosh, S., et al. Dimensional crossover of thermal transport in few-layer graphene. *Nat. Mater.* **9**,
360 555 (2010).
361 44. Gu, X., Li, B. & Yang, R. Layer thickness-dependent phonon properties and thermal conductivity
362 of MoS_2. *J. Appl. Phys.* **119**, 085106 (2016).
363 45. Kresse, G. & Hafner, J. Ab-initio molecular-dynamics for open-shell transition-metals. *Phys. Rev.*
364 *B* **48**, 13115-13118 (1993).
365 46. Kresse, G. & Furthmuller, J. Efficient iterative schemes for ab initio total-energy calculations
366 using a plane-wave basis set. *Phys. Rev. B* **54**, 11169-11186 (1996).
367 47. Perdew, J. P. & Zunger, A. Self-interaction correction to density-functional approximations for
368 many-electron systems. *Phys. Rev. B* **23**, 5048-5079 (1981).
369 48. Blochl, P. E. Projector augmented-wave method. *Phys. Rev. B* **50**, 17953-17979 (1994).
370 49. Kresse, G. & Joubert, D. From ultrasoft pseudopotentials to the projector augmented-wave
371 method. *Phys. Rev. B* **59**, 1758-1775 (1999).
372 50. Togo, A. & Tanaka, I. First principles phonon calculations in materials science. *Scripta Mater.*
373 **108**, 1-5 (2015).
374 51. Mizokami, K., Togo, A. & Tanaka, I. Lattice thermal conductivities of two SiO_2 polymorphs by
375 first-principles calculations and the phonon boltzmann transport equation. *Phys. Rev. B* **97**, 224306
376 (2018).
377 52. Togo, A., Chaput, L. & Tanaka, I. Distributions of phonon lifetimes in brillouin zones. *Phys. Rev.*
378 *B* **91**, 094306 (2015).
379